

RUSSIAN ACADEMY OF SCIENCES  
PETERSBURG NUCLEAR PHYSICS INSTITUTE

# High-Precision Temperature Measuring Instrument

P.Kravtsov, V.Trofimov, A.Martyushov

Gatchina 2006

## **Высокоточный прибор для измерения температуры**

П. А. Кравцов, В. А. Трофимов, А. А. Мартюшов

### **А н н о т а ц и я**

Описано устройство и основные принципы работы прибора для измерения температуры с высокой точностью. Прибор обеспечивает подключение до восьми датчиков температуры резистивного или полупроводникового типа. Разрешение прибора составляет 2 мкВ, что соответствует температуре 0.005 К для термометра сопротивления Pt-100. В приборе реализован метод подавления влияния термо-ЭДС с помощью усреднения с реверсом измерительного тока. Проведены испытания прибора на специально созданном стенде для исследования влияния термо-ЭДС. Описаны результаты испытаний прибора и опыт его применения.

### **Abstract**

A high-precision device is described intended for the temperature measurements. It provides reading of up to 8 temperature sensors of resistive or semiconductor type. The device resolution is 2  $\mu$ V that corresponds to the temperature 0.005 K for the Pt-100 sensor. A special method is implemented in the device to suppress the thermo EMF influence using the averaging with reverse of the measuring current. A dedicated experimental setup was built to investigate the measurement noise and the thermal electromotive force influence. The results of the device tests are described along with operating experience.

## Introduction

Cryogenic systems always require temperature measurement. Usually these measurements are done using the Resistance Temperature Detectors (RTD) or the semiconductor cryogenic temperature sensors. The error of the temperature measurements consists of a calibration error and a measurement error. The best absolute calibration error of the commercial temperature sensors is about 5 mK [1]. Generally a cheap uncalibrated commercial sensor could be easily standardized using the boiling temperature and the triple point of various cryogenic liquids. The measurement error is caused by the signal noise and drift in the measurement device.

The thermal electromotive force at connector contacts and other joints becomes significant for the cryogenic sensor measurements, because of the low signal from the sensor itself and wide temperature region of the joints. This thermal electromotive voltage appears in all heterogeneous joints and depends on the temperature. Even copper-copper joint made from various wire manufacturers may result in thermoelectric voltage of  $0.2 \mu\text{V}/^\circ\text{C}$ . The resistor itself can generate thermoelectric voltage due to joints of resistor material and its leads. This voltage varies from  $20 \mu\text{V}/^\circ\text{C}$  for usual metal film resistors to  $400 \mu\text{V}/^\circ\text{C}$  for carbon composition resistors [2]. This signal is negligible if both resistor leads are kept at the same temperature. But even  $1^\circ\text{C}$  difference between the leads temperature gives sensor signal offset of  $20 \mu\text{V}$  that is crucial for the precision temperature measurements.

Traditional methods of precision maintenance at the microvolt level include using of the 4-wire connection for the resistive sensor, minimizing of the thermocouple joints and the temperature gradients, balancing of the thermocouple joints for both supply and return wires of the differential signal [3]. These techniques are difficult for the cryogenic systems. A typical connection circuit of a temperature sensor for the cryogenic system includes at least two connectors (at a measuring instrument and at vacuum connector) and a number of soldering. Besides, some contacts of the circuit have different temperatures. The wires also have variable temperature because of heat flux through the wire.

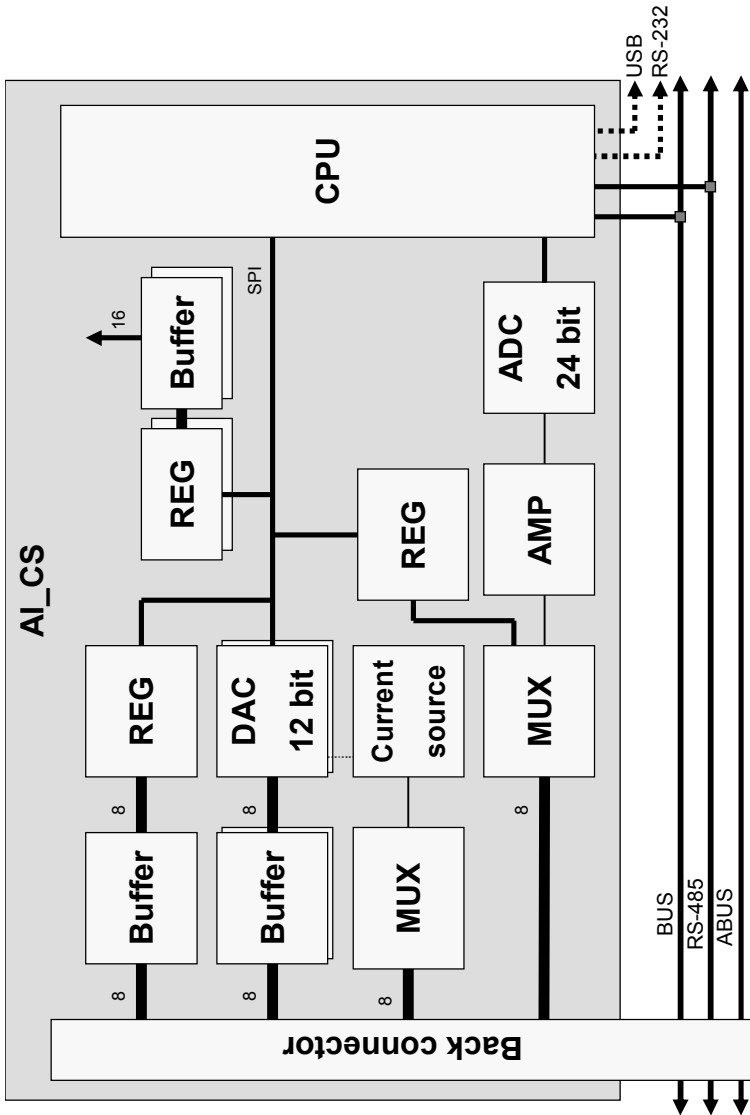


Fig. 1. AI\_CS simplified diagram.

A special device (AI\_CS) was developed for the precision temperature measurements using the RTD or semiconductor temperature sensors with special reversible current supply. The measurement procedure implemented in the device allows for precision keeping with elimination of the thermoelectric voltage influence due to averaging of the direct and reverse current signal. A dedicated experimental setup was built to investigate the measurement noise and the thermal electromotive force influence.

## General layout of the device

AI\_CS device (Fig. 1) is designed for resistive sensors measurements. It is equipped with programmable reversible current supply of high stability and the range of  $10\ \mu\text{A}\div 3\ \text{mA}$ . This is usual measurement current range either for the Resistance Temperature Detectors (RTD), like Pt-100 or Pt-1000; or for the semiconductor cryogenic temperature sensors like germanium or silicon diodes. Current supply could be adjusted manually using the stable resistive divider or programmed by CPU using one of the onboard DAC channels. The current from the current source is supplied to the sensor using eight channels multiplexer<sup>1</sup>. Voltage signals from the sensor are multiplexed using similar eight channels differential multiplexer<sup>2</sup>, buffered in amplifier<sup>3</sup> and converted using the 24-bit ADC<sup>4</sup>. All analog signals are routed through the back connector<sup>5</sup>. Analog input channels also allow the current shunt installation for working with the current output sensors ( $0\div 20\ \text{mA}$ ).

The device is equipped with eight analog output channels from two 4-channel 12-bit DACs<sup>6</sup> that are buffered and amplified in the quad high precision operational amplifiers<sup>7</sup>. One of these analog output channels

---

<sup>1</sup> MAX367, Maxim Integrated Products.

<sup>2</sup> MPC507, Burr-Brown products, Texas Instruments Incorporated.

<sup>3</sup> AD620 instrumentation amplifier, Analog Devices Inc.

<sup>4</sup> LTC2440, Linear Technology Corporation.

<sup>5</sup> DIN C 96-pin connector.

<sup>6</sup> DAC7615, Burr-Brown products, Texas Instruments Incorporated.

<sup>7</sup> OPA4277, Burr-Brown products, Texas Instruments Incorporated.

could be used for the current source control. All eight signals are connected through the back connector. Also, 24 buffered digital outputs are provided for the actuating devices control like valves or compressors. Eight of them are routed to the back connector and 16 – to the separate connector at the front of the device.

The device is controlled by a high speed 8051-family CPU<sup>8</sup> with 8 kB of in-system programmable flash memory and 1 kB of data memory, working at 22.1184 MHz. There are several options (selectable by onboard jumpers) of communication interface: USB, RS-232 serial interface, full-duplex RS-485 serial interface, internal serial bus interface. The internal bus interface is used for the data exchange with the crate controller during the crate mode working with other devices in the crate. The AI\_CS instrument is developed in the standard EURO 100 x 160 mm module size.

The firmware for the AI\_CS device was written in C language and provides all basic operations like reading the ADC, control the DAC signals and digital output drivers, and data exchange via communication interface. A Proportional-Integral-Derivative (PID) regulation algorithm was implemented in the firmware independently for every channel allowing for controlling the particular DAC signal using the selected ADC channel.

**Current supply**

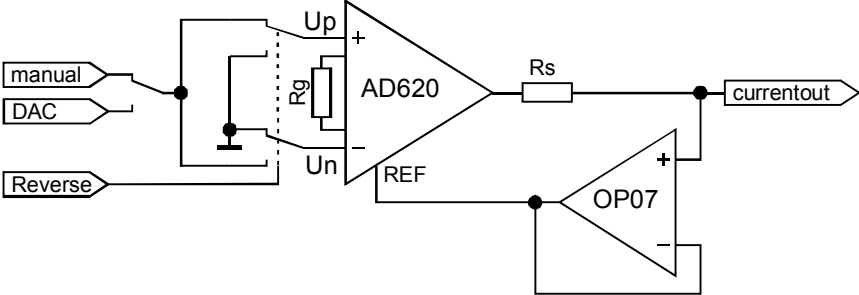


Fig. 2. Reversible current supply.

<sup>8</sup> C8051F314, Silicon Laboratories Inc.

The current supply was developed on the basis of an instrumentation amplifier<sup>9</sup> and an operational amplifier<sup>10</sup> (Fig. 2). The operational amplifier (OP07) buffers the reference terminal of the instrumentation amplifier (AD620). The reference terminal potential defines the zero output voltage of the AD620. It provides a direct means of injecting a precise offset to the output. Thus, the output voltage of the AD620 appears across the current shunt  $R_s$ , which converts it to a current. This current, less only the input bias current of the operational amplifier ( $\pm 1.2$  nA), then flows out to the load. The current could be calculated using the formula:  $I = G \cdot (U_p - U_n) / R_s$ , where  $G$  is the amplifier gain defined by the  $R_g$  resistor:  $G = 49.4 \text{ k}\Omega / R_g + 1$ . For the most applications,  $G = 1$  is selected and the  $R_G$  pins are unconnected.

A four channel multiplexer<sup>11</sup> was used for the switching the input signals of the instrumentation amplifier. It is controlled by “Reverse” signal and enables switching of the direct and the reverse current to the load. The current control signal could be selected from manual reference or one of the onboard DAC signals for the automatic current control. The current stability of the source is about 10 ppm/°C as a result of shunt resistor and reference voltage stability.

## Measurements noise

AI\_CS device provides 8 channels for the RTD sensors connection. Each sensor is connected using 4-wire scheme to the back connector (Fig. 3, channel 1). The current is supplied to the sensor through the multiplexer ( $I_{pos}$  in the diagram) from the reversible current source. The use of direct and reverse currents with averaging of the voltage signals makes it possible to suppress the influence of thermoelectromotive force at connectors and other joints that becomes very important for the cryogenic sensor measurements. Voltage signal ( $U_{pos}$  and  $U_{neg}$  in the diagram) from the sensor is amplified and measured in differential mode. The

---

<sup>9</sup> AD620 instrumentation amplifier, Analog Devices Inc.

<sup>10</sup> OP07, Burr-Brown products, Texas Instruments Incorporated.

<sup>11</sup> MPC509, Burr-Brown products, Texas Instruments Incorporated.

measured values for both current directions are  $U^+ = U_S + \xi$  and  $U^- = -U_S + \xi$ , where  $U_S$  is authentic sensor voltage and  $\xi$  – thermoelectromotive voltage that always has the same polarity defined by contact materials. Thus, the true sensor voltage could be calculated using the formula:  $U_S = \frac{U^+ - U^-}{2}$ .

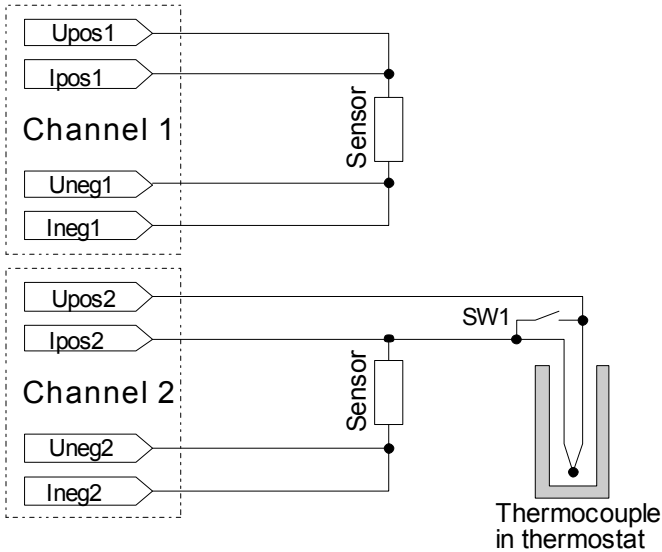


Fig. 3. Connection diagram of usual sensor (channel 1) and sensor with thermocouple (channel 2).

A special scheme was assembled for the checking of the AI\_CS device measurement noise and stability (Fig. 3, channel 2). A thermocouple was connected serially to the  $U_{pos}$  signal of the second AI\_CS channel for imitation of the thermoelectromotive voltage. The thermocouple was placed in the thermostat to extend the range of the voltage addition to  $0 \div 2.25$  mV that corresponds to temperature range of  $298 \div 260$  K. Both sensors in channel 1 and channel 2 were imitated by the stable 100 Ohm resistors with accuracy of 0.1 % and temperature

coefficient of 10 ppm/K. There is also a possibility to short the thermocouple using the SW1 switch.

First measurement was done with usual procedure without averaging (Fig. 4). Channel 2 curve neatly tracks changing of the thermocouple voltage during cooling and heating of the thermocouple. Channel 1 curve also tracks ambient temperature in the room, through the influence of the thermoelectromotive voltage. This results in poor stability of the sensor 1 signal (Fig. 5).

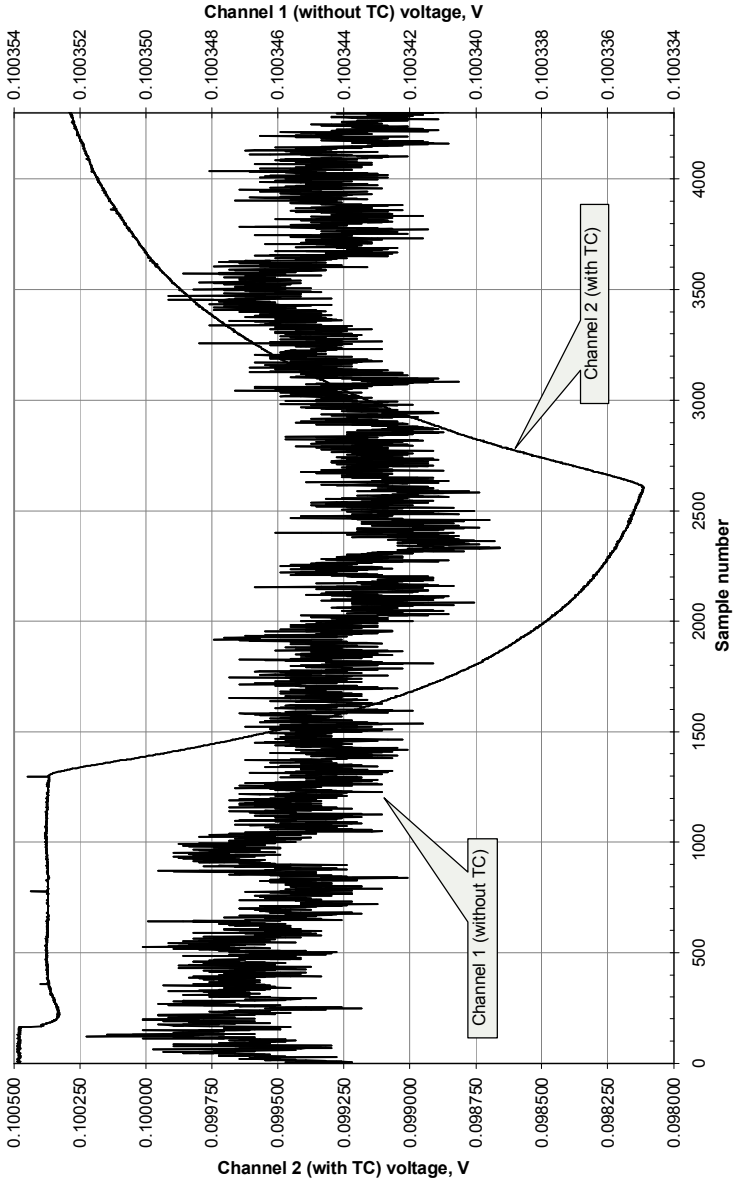


Fig. 4. Cooling and heating of the thermocouple without averaging.

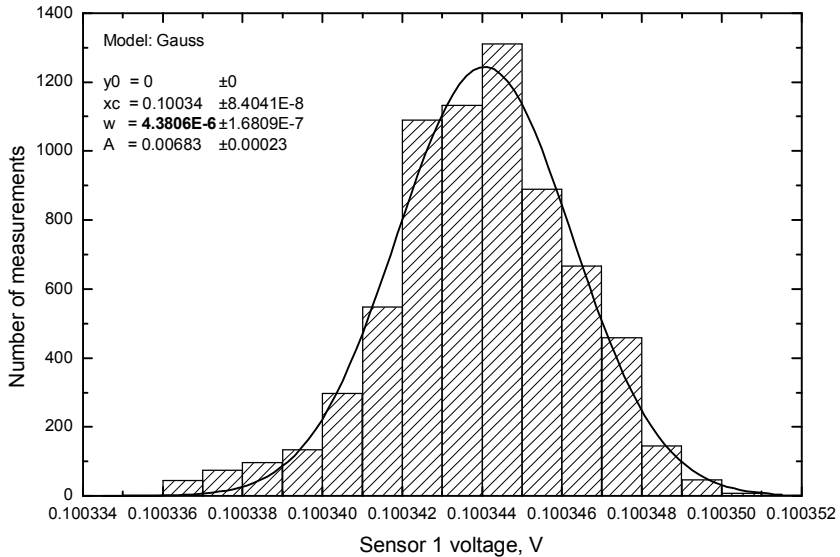


Fig. 5. Signal distribution for channel 1 without averaging.

Second measurement was carried out with the current reverse and the averaging of two ADC samples (direct and reverse current samples). The same temperature cycle of the thermocouple was reproduced with cooling from room temperature (298 K) down to 260 K and subsequent heating up to room temperature. Obviously, sensor 2 curve does not track change of the thermocouple voltage with temperature (Fig. 6). Quite the contrary, signal is stable at the level of some 100 mV because thermocouple influence in the range of 0÷2.25 mV is subtracted in the averaging procedure. Figure also shows that signal distribution for the sensor with thermocouple is significantly wider, becoming almost equal after shorting the thermocouple (right part of the chart in Fig. 6).

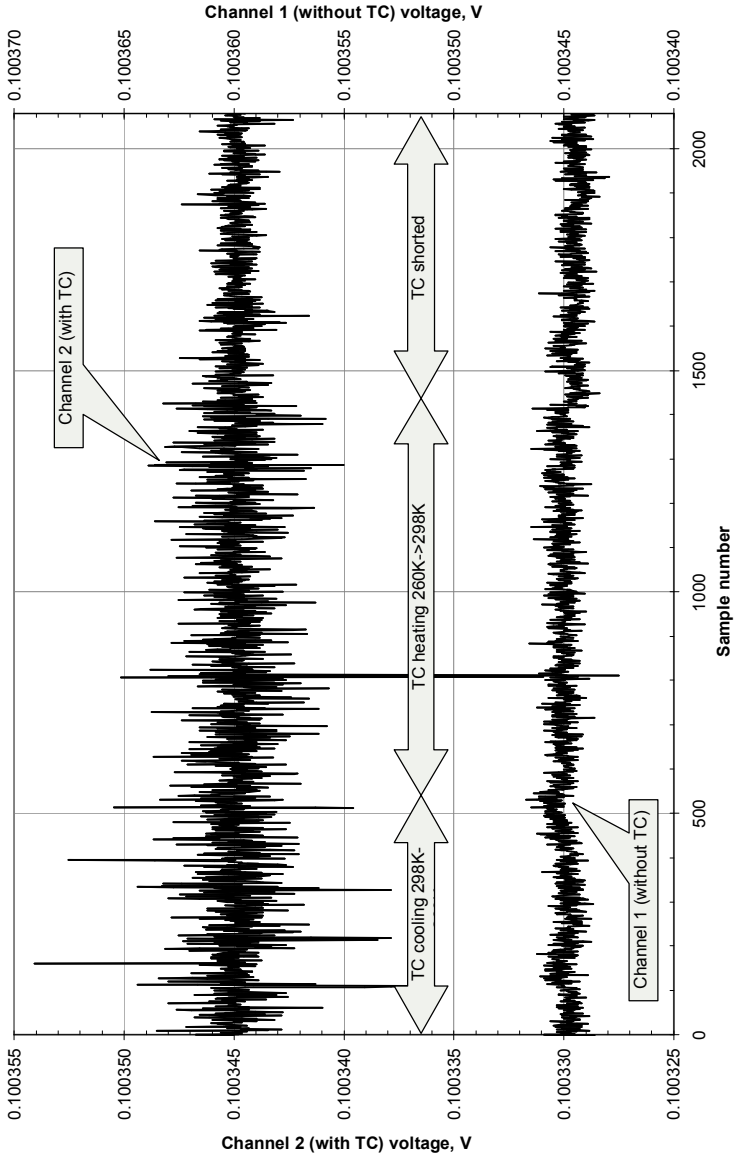


Fig. 6. Cooling and heating of the thermocouple with averaging of direct and reverse current measurements.

Sensor signal distributions (Fig. 7) demonstrate much smaller widths than without averaging. Averaging of two ADC samples measured with opposite current directions improves the signal distribution width by a factor of 3.6 ( $1.22 \mu\text{V}$  instead of  $4.38 \mu\text{V}$ ) for the channel 1 (without thermocouple). It also makes possible to calculate the signal distribution width for the channel 2, because without averaging this channel drifted by  $2.25 \text{ mV}$  during temperature cycle. There is still small influence of the thermocouple temperature cycle to the signal distribution width ( $2.03 \mu\text{V}$ ) that is almost vanished after shorten the thermocouple with switch SW1 ( $1.35 \mu\text{V}$  is very similar to  $1.22 \mu\text{V}$  width of channel 1). Thus, the averaging has a great effect on the signal distribution of sensor with thermocouple, improving the distribution width by 3 orders of magnitude from  $2.25 \text{ mV}$  to  $2.03 \mu\text{V}$ .

The long-term behavior of both sensor signals is also very stable (Fig. 8). During three hours all channels were measured with direct/reverse current averaging. Thermocouple was exposed to room temperature and connected to the sensor 2. This lead to slightly wider signal distribution of sensor 2 ( $1.93 \mu\text{V}$ ) in comparison with sensor 1 ( $1.19 \mu\text{V}$ ) that sensed only thermoelectromotive voltage at connectors and solder joints.

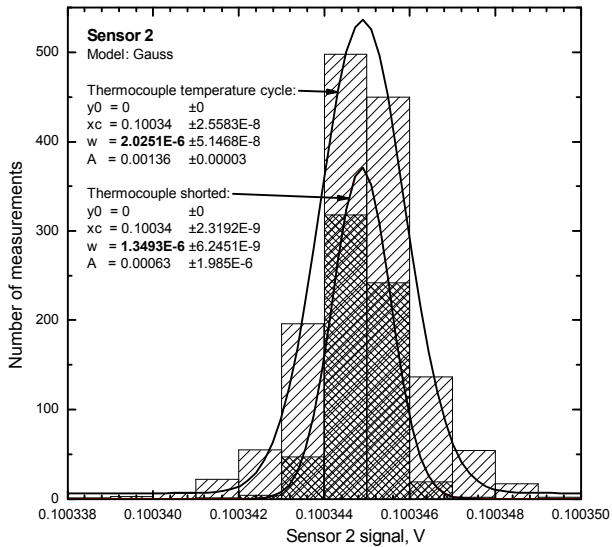
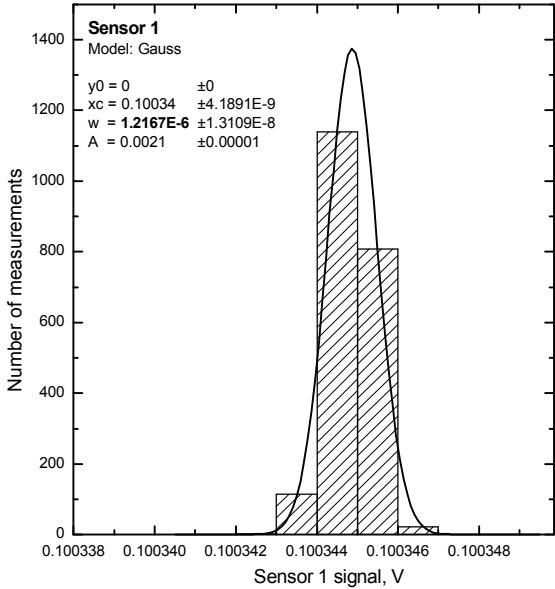


Fig. 7. Sensor signals distributions with direct and reverse current averaging.

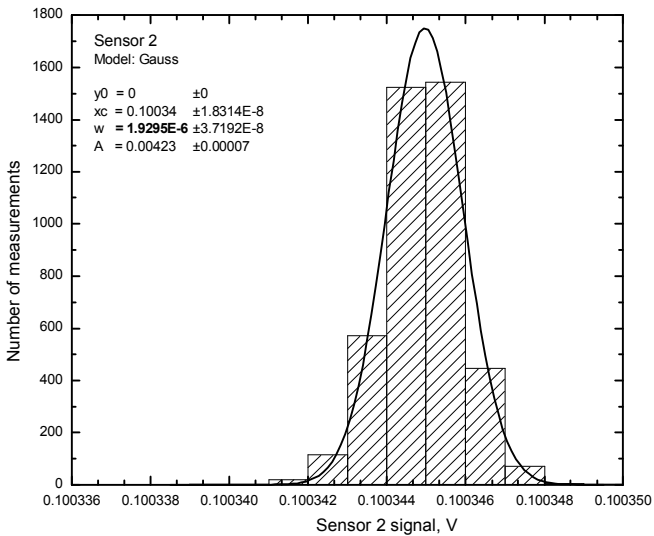
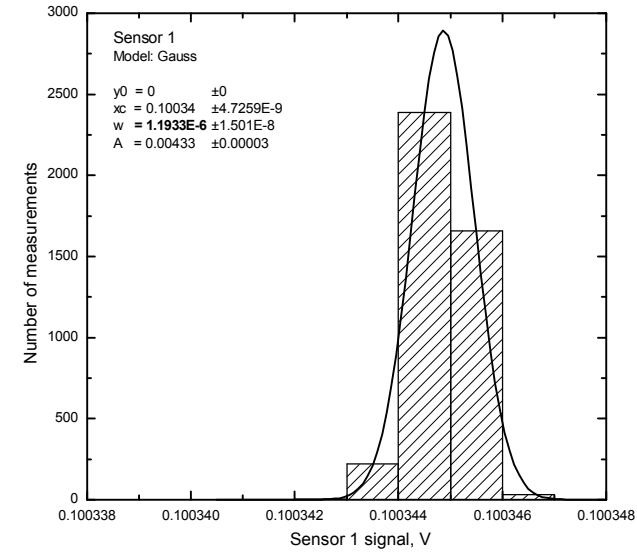


Fig. 8. Signal distributions for three hours measurement.

Finally, the stable resistor gives the measurement noise of about  $2\ \mu\text{V}$  peak to peak with signal distribution width of  $1.19\ \mu\text{V}$ . This corresponds to the absolute calibration error of about  $2\ \mu\text{V}$  described below.

## Calibration

AI\_CS device was calibrated using Keithley 2700 digital multimeter (KDMM). For each setpoint of current source three voltages were measured: ADC sample with averaging of direct and reverse current and two Keithley readings for direct and reverse current. Keithley samples were averaged afterwards and data were interpolated with linear regression. The difference between average Keithley reading and voltage calculated by calibration is shown in Fig. 9. Calibration error is low enough in the range of  $0\div 160\ \text{mV}$  that corresponds to the temperature range of  $10\div 430\ \text{K}$  measured by Pt-100 sensor (grayed area in the chart). The deviation in this region is about  $2\ \mu\text{V}$  and is lower than Keithley digital multimeter error ( $6\div 9\ \mu\text{V}$ ). Thus, the Keithley multimeter error can be assumed for the total error of the device. In the temperature scale of Pt-100 sensor the calibration error is about  $0.02\ \text{K}$  with resolution of less than  $0.005\ \text{K}$ .

The device was also calibrated for the measurements without averaging. This calibration shows reasonable error in the whole range of the sensor voltage (Fig. 10). The increase of the calibration error for the averaged measurements at the voltages more than  $160\ \text{mV}$  is connected with the ADC error for negative voltage samples. This growth disappears for the measurements without averaging. Both modes are acceptable for most of the resistive or semiconductor sensors. The calibration dependencies were implemented in the device firmware for both measurement modes.

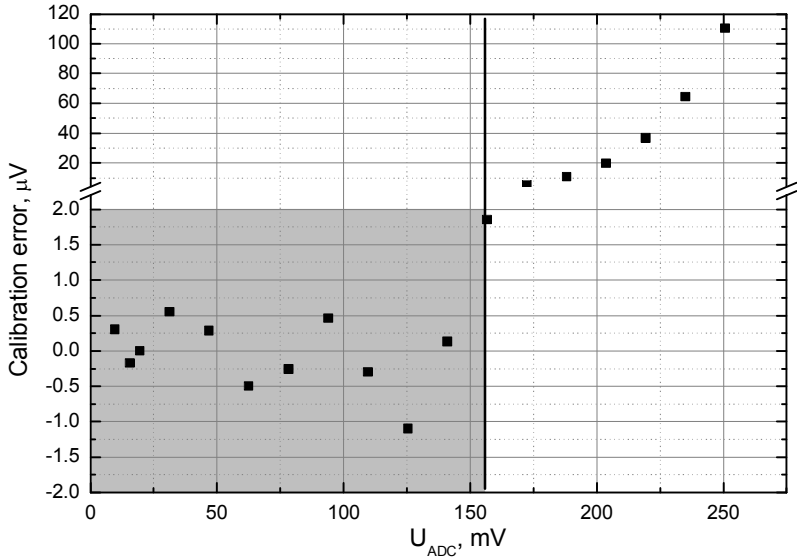


Fig. 9. Calibration error of the averaged measurements.

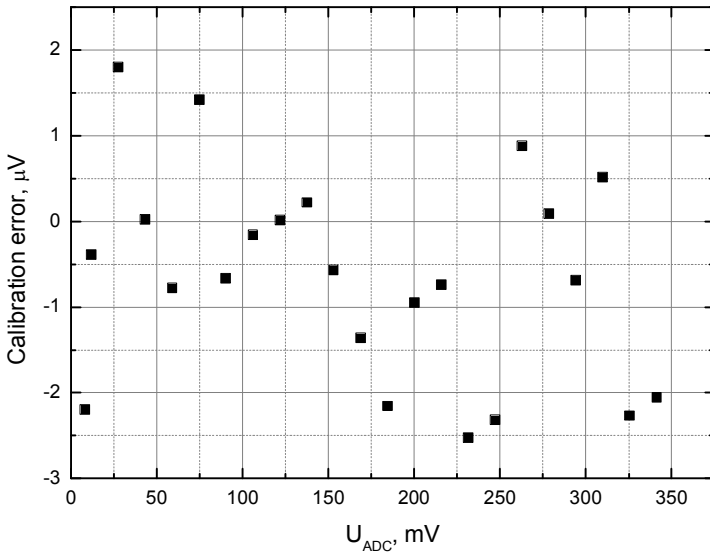


Fig. 10. Calibration error without averaging.

## High speed measurements

The ADC of the device provides selectable sampling speed in the range of 6.875 Hz÷3.52 kHz. Declared RMS noise of the ADC changed from 200 nV to 23  $\mu$ V respectively. Besides, it has automatic 50/60 Hz noise rejection for the lowest sampling speed. The measurement noise tests and calibration were carried out at the lowest ADC speed (6.875 Hz) with highest precision. This leads to total 8 channels measurement time of 2.4 s and 1.2 s with and without averaging, correspondingly.

The device was also tested with higher ADC sampling speed. Fig. 11 shows the signal distribution of channel 1 (stable resistor, see connection diagram in Fig. 3) at 110 Hz ADC speed. Measurements were done with averaging of the signals for direct and reverse currents. With moderate increase of the distribution width (2.7  $\mu$ V instead of 1.2  $\mu$ V for lowest ADC speed), this speed essentially improves the total measurement time of the 8 channels: 140 ms with averaging. The distribution width is still on the level of calibration error.

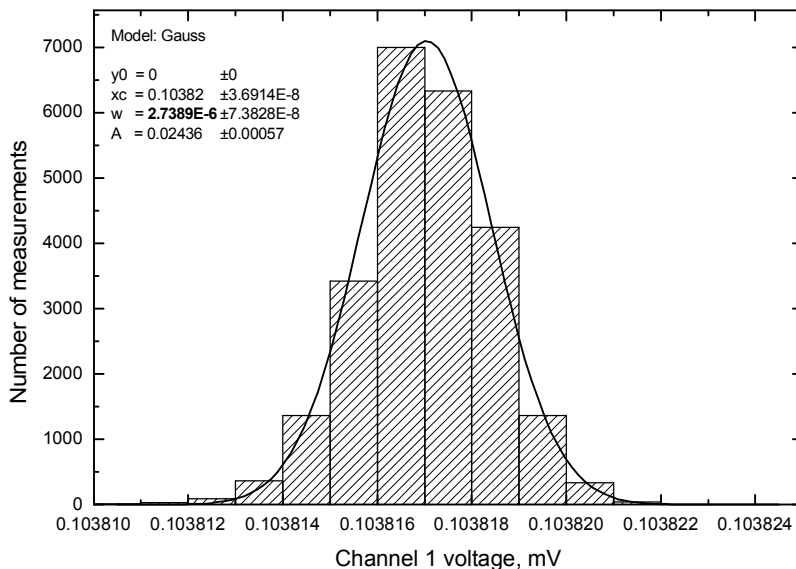


Fig. 11. Sensor 1 signal distribution at 110 Hz sampling rate with averaging.

Signal distribution for the 220 Hz sampling speed (Fig. 12) also shows acceptable result. The distribution width for the 220Hz measurement with averaging ( $3.8 \mu\text{V}$ ) is less than for the 6.9 Hz without averaging ( $4.4 \mu\text{V}$  – see Fig. 5). With reduced sensitivity of the device, it is still less than calibration error of about  $6 \mu\text{V}$ . The total measurement time of the 8 channels is 75 ms with averaging.

Thus, the averaging procedure of the signals with direct and reverse currents allows essentially accelerate the measurements with acceptable loss of the sensitivity. Table summarizes the total measurement time for various modes along with sensitivity for averaged measurements (signal distribution width).

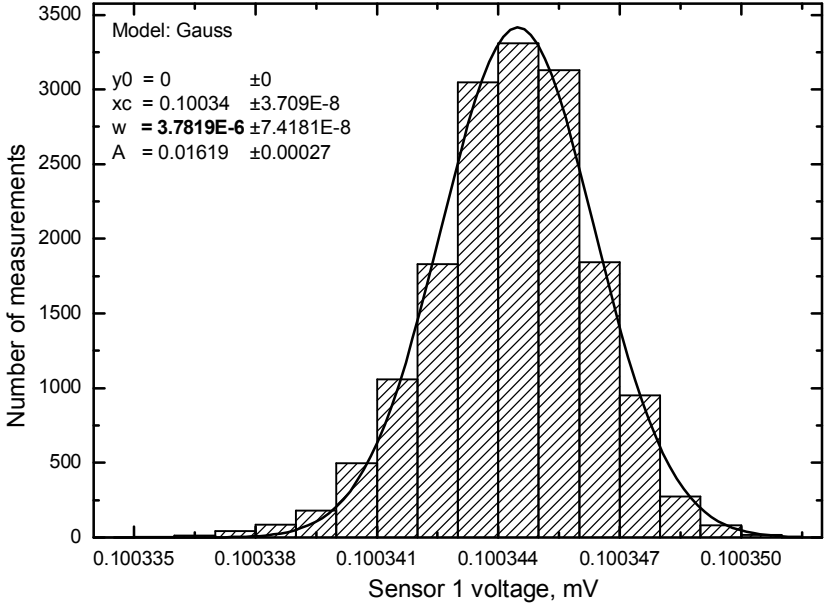


Fig. 12. Sensor 1 signal distribution at 220 Hz sampling rate with averaging.

*Table.*

Total measurement time for various modes.

ADC speed, Hz	Sensitivity, $\mu\text{V}$ (with averaging)	Total measurement time for 8 channels, ms	
		With averaging	Without averaging
6.875	1.2	2400	1200
55	2.3	290	143
110	2.7	140	69
220	3.8	75	36

## Operating experience

The AI\_CS device was used in the Deuterium Removal Unit (DRU) [4] of the MuCap experiment. It provides the temperature measurements with Pt-100 sensors and stabilization using the two heaters. The sensors were calibrated by hydrogen triple point. The device proved to be very reliable and flexible during DRU experiments.

The moisture calibration system for the MuCap experiment also utilizes the AI\_CS device for the temperature stabilization. The device provides the measurements of a temperature sensor (Pt-100), two pressure sensors, and a dew-point transmitter. The system comprises of closed working vessel filled with Xenon that is cooled through a heat bridge that is connected to the liquid nitrogen tank. The heat bridge is equipped with the electrical heater mounted near the working vessel for the temperature stabilization. Heater power supply is controlled by the AI\_CS device with voltage and current monitor signals being measured.

Temperature of the working vessel of the system could be stabilized using PID regulation with the feedback from Pt-100 sensor or pressure sensor. Typical temperature behavior is shown in Fig. 13. Temperature distribution for over 18 hours experiment indicates the stability of the temperature better than  $\pm 0.01$  K.

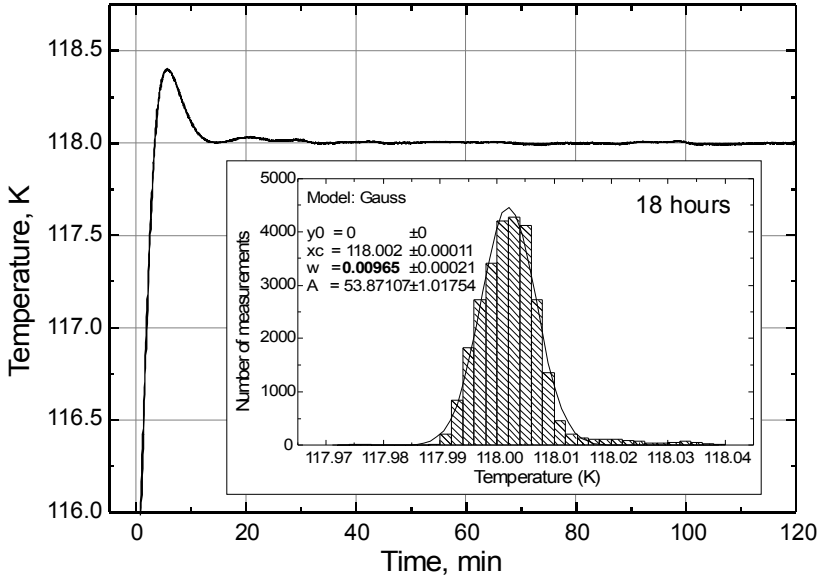


Fig. 13. Temperature stabilization using onboard PID regulation algorithm.

## Conclusion

The AI\_CS instrument proved to be very stable and reliable during the cryogenic systems experiments. With regard to the measurement precision, it achieved very good result for the resolution ( $2 \mu\text{V}$  or  $0.005 \text{ K}$  for Pt-100 sensor), which is comparable to the calibration error of the best commercial temperature sensors. A special method implemented in the device to suppress the thermo EMF influence distinctly improves the instrument resolution.

The flexibility of the instrument allows one to connect usual sensors with voltage or current output. Using of the microprocessor core enables the implementation of additional control algorithms in the device, allowing stand-alone mode of system control operation. The control operation is also supported with abundance of analog and digital control

channels. Variety of the data exchange interfaces simplifies connection of the instrument to the external control system or computer.

## Acknowledgments

The authors wish to thank Dr. A. Vasilyev for important design remarks and fruitful discussions. They gratefully acknowledge the MuCap collaboration for their support of the experiments involving the AI\_CS instrument.

## References

- [1] Sensor Calibration Accuracies, Lake Shore Cryotronics, Inc. <http://www.lakeshore.com>.
- [2] RCD Components Inc., 520 E. Industrial Park Drive, Manchester NH, 03109, <http://www.rcd-comp.com>.
- [3] D. Grant, S. Wurcer. Avoiding Passive-Component Pitfalls. Analog Dialogue **17-2** (1983).
- [4] I. Alekseev *et al.* Experimental Results of Hydrogen Distillation at the Deuterium Removal Unit of the MuCap Experiment. Preprint PNPI-2702, Gatchina (2006) 26 p.